

CMS Physics Analysis Summary

Contact: cms-pag-conveners-higgs@cern.ch

2018/06/03

Search for the $tH(H \rightarrow b\bar{b})$ process in pp collisions at $\sqrt{s} = 13 \text{ TeV}$ and study of Higgs boson couplings

The CMS Collaboration

Abstract

A search for the production of a Higgs boson in association with a single top quark (tH) is presented. The analysis focuses on Higgs boson decays to bottom quark-antiquark pairs and leptonic top quark decays. The full data set of pp collisions recorded by the CMS detector in 2016 at a center-of-mass energy of 13 TeV , corresponding to an integrated luminosity of 35.9 fb^{-1} , is analyzed. A multivariate classifier is used to discriminate signal candidates from the overwhelming background processes. Several scenarios for varied strength of the coupling of the Higgs boson to top quarks and to vector bosons are examined and limits on the combined cross section for Higgs boson production, either in association with a pair of top quarks or a single top quark, are derived. In addition, limits on the signal strength of Higgs boson production in association with a single top quark are set for two specific cases. The observed (expected) limit for tH production in the standard model is 89.5 (41.4) times the predicted cross section. In case of an inverted top-Higgs coupling, the observed (expected) limit is 5.83 (2.94) times the prediction.

1 Introduction

Since the discovery of a Higgs boson-like particle by the ATLAS and the CMS experiments in 2012 [1, 2], it has been a crucial task to measure the properties of this new particle precisely and to determine whether they are in agreement with the predictions of the standard model of particle physics (SM). The strength of the Yukawa coupling y_t of the Higgs boson to the heaviest particle of the SM, the top quark, plays a very important role in this verification process. Deviations in this parameter from the SM prediction could be evidence for physics beyond the standard model (BSM) and therefore make it essential to extract the most accurate value from the data.

Recently, the production of a Higgs boson in association with a pair of top quarks ($t\bar{t}H$) has been observed by the CMS Collaboration [3]. This measurement is the first direct observation of the coupling of the Higgs boson to the top quark. $t\bar{t}H$ production shows a high sensitivity to the magnitude of y_t , however, it cannot provide any information about the sign of y_t , as it depends on $|y_t|^2$. Some processes, such as the decay of a Higgs boson into a photon pair [4] or the associated production of a Higgs boson and a Z boson via gluon-gluon fusion [5], are sensitive to the sign of y_t , but current measurements only disfavor $y_t < 0$ without excluding it [6–8]. However, these constraints are made under the assumption of no BSM particles inside the corresponding loop diagrams [9].

A way to resolve this degeneracy in the sign of y_t is to search for the associated production of a Higgs boson with single top quarks (tH) in pp collisions. As for the more common case without the Higgs boson, single top quark production can be separated at leading order (LO) into three production modes: t channel (hereafter referred to as "tHQ"), tW -associated production (hereafter referred to as "tHW"), and s channel. As the s -channel production mode has a negligible cross section at the LHC [10], only the other two modes are considered in this search. Both in the tHQ and tHW channels, the Higgs boson can couple either to the top quark or to the W boson as can be seen in the Feynman graphs in Fig. 1. A way to parametrize the couplings of the Higgs boson to the SM particles is given by using the values κ_t and κ_V , which are defined as the ratio of the actual coupling strengths to the SM predictions for the top quark and the massive vector bosons, respectively. Since both diagrams in each channel have the same final state, these processes interfere with each other and the resulting amplitude strongly depends on the values of κ_t , κ_V , and the relative sign between both. Therefore, tH production is the only process to probe the relative sign of the couplings in Higgs boson production rather than in Higgs boson decays.

In the SM case, where κ_t and κ_V are both equal to +1, this interference is maximally destructive and the cross sections, calculated using MG5_aMC@NLO [11] and the method described in Ref. [10], are 71 fb for tHQ and 16 fb for tHW at 13 TeV center-of-mass energy. For values of $\kappa_t < 0$, while still demanding $\kappa_V > 0$, the interference becomes constructive and enhances the cross section and changes the kinematic quantities of the events. The impact on the cross section due to variations of the coupling strengths is illustrated in Fig. 2. The scenario with a SM Higgs boson coupling to vector bosons ($\kappa_V = +1$), but a flipped sign for the top-Yukawa coupling ($\kappa_t = -1$), will be called the *inverted top coupling* (ITC) scenario in the following. Assuming this scenario, the cross section for tHQ (tHW) is 739 fb (147 fb) at 13 TeV center-of-mass energy.

Even in the case of an enhanced cross section, tH production is swamped by events from background processes featuring similar final-state signatures. The dominating background contribution comes from $t\bar{t}$ production with additional jets, followed by single top quark production. Multivariate techniques are therefore brought to use for the search for the production of a Higgs

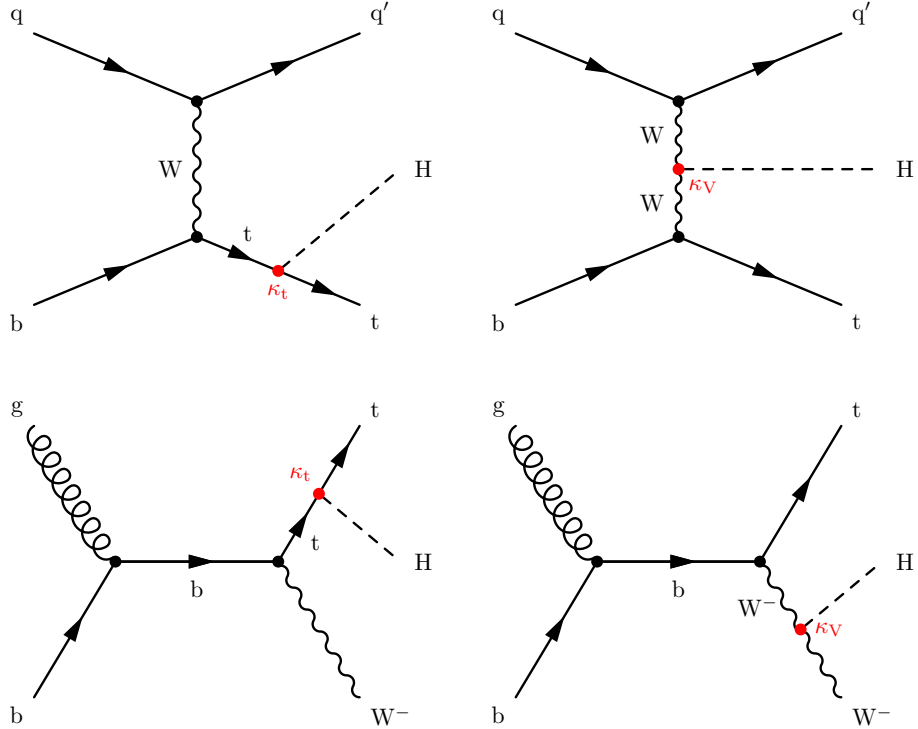


Figure 1: Representative Feynman diagrams for the associated production of single top quarks and Higgs bosons in the t channel (top row) and in the tW channel (bottom row). The Higgs boson can couple either to the top quark or the W boson in both processes.

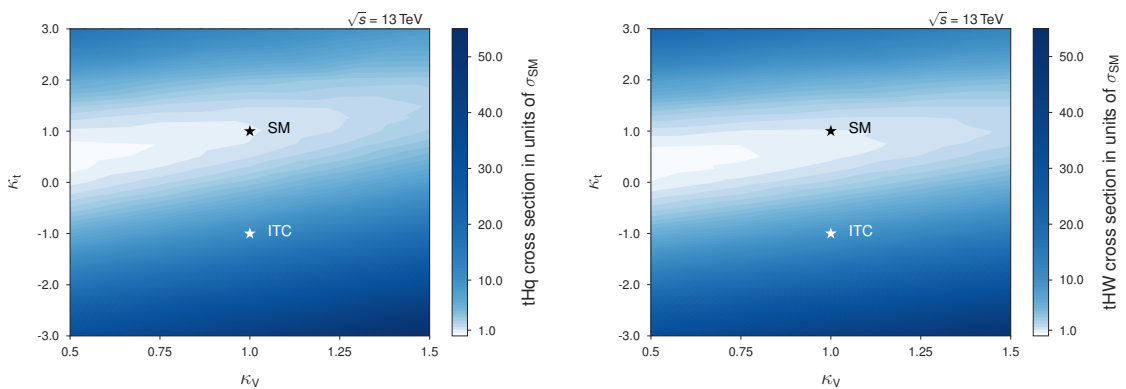


Figure 2: Cross sections in the $\kappa_t - \kappa_V$ plane at 13 TeV for tHq (left) and tHW (right) production. Right figure adapted from [12].

boson in association with a single top quark using the data set of proton-proton collisions at a center-of-mass energy of 13 TeV, collected by the CMS detector in 2016. The analyzed data correspond to an integrated luminosity of 35.9 fb^{-1} . The analysis sets limits on the cross section times branching ratio for this process in two specific scenarios: for a top-Higgs coupling as predicted by the SM and for the ITC scenario. In addition, the coupling of the Higgs boson to the top quark is studied in a more general way by exploring a full range of the coupling modifier ratios κ_t/κ_V and setting upper limits on the combined cross section times branching ratio for the Higgs boson production in association with single top quarks and top quark-antiquark pairs.

2 Event simulation

Different Monte Carlo event generators are used for the simulation of signal and background processes. The signal samples of the tHq and the tHW production processes are simulated using MG5_aMC@NLO [11] at LO precision in perturbative quantum chromodynamics (QCD) and the NNPDF3.0 PDF set [13]. Both samples are generated for the ITC case with unit weights and the remaining scenarios for the different κ_t/κ_V ratio combinations are obtained by the application of event-dependent weights that account for the difference in the kinematics. The values for κ_t range from -3 to $+3$ and for κ_V from $+0.5$ to $+1.5$. The tHq process is generated within the four-flavor scheme and with dynamical factorization and renormalization scales, while for the generation of tHW events, fixed scales (40 GeV) and the five-flavor scheme are used, which is motivated by the need to avoid interference with the tH production at leading order.

In all simulations, a Higgs boson mass of 125 GeV and a top quark mass of 172.5 GeV are used and the parton shower modeling for all samples is done using PYTHIA 8 [14]. The main backgrounds from $t\bar{t}$ production as well as from $t\bar{t}H$ and single top quark production are simulated using the POWHEG event generator [15–17]. The production of $t\bar{t}$ in association with a W boson ($t\bar{t}W$) or a Z boson ($t\bar{t}Z$) is simulated using MG5_aMC@NLO. The production of Z+jets events is simulated using MG5_aMC@NLO and the FxFx merging scheme [18].

To account for the effect of additional proton-proton interactions (pileup), the event generator POWHEG is used to simulate superimposed minimum-bias events with in-time and out-of-time pileup contributions with the same distribution as observed in data. In a final step each generated event undergoes a full CMS detector simulation based on GEANT 4 [19, 20] and is reconstructed using the same algorithms as for data.

3 Object definitions and event selections

3.1 Object definitions

The particle-flow (PF) algorithm [21] aims to reconstruct and identify each individual particle in an event, with an optimized combination of information from the various elements of the CMS detector. The energy of photons is directly obtained from the ECAL measurement, corrected for zero-suppression effects. The energy of electrons is determined from a combination of the electron momentum at the primary interaction vertex as determined by the tracker, the energy of the corresponding ECAL cluster, and the energy sum of all bremsstrahlung photons spatially compatible with originating from the electron track. The energy of muons is obtained from the curvature of the corresponding track. The energy of charged hadrons is determined from a combination of their momentum measured in the tracker and the matching ECAL and

HCAL energy deposits, corrected for zero-suppression effects and for the response function of the calorimeters to hadronic showers. Finally, the energy of neutral hadrons is obtained from the corresponding corrected ECAL and HCAL energy. Jets are clustered from PF objects, using the anti- k_T algorithm with a distance parameter of 0.4 [22]. The measured jet energy is corrected in data and simulated events to account for pileup interactions and known detector effects [23]. The energy resolution of simulated jets is modified to model the jet energy resolution observed in data. The identification of jets that originate from the hadronization of b quarks is essential for this analysis as four b quarks exist in the final state of the signal process. The CSVv2 b tagging algorithm [24] is used at its medium working point for the identification of b jets. This working point provides a tagging efficiency of about 69% for b jets and a misidentification probability of approximately 1% for light-flavored jets or jets from gluons. Scale factors are applied to the distribution of the simulated events to correct the b-tag classifier output distributions for differences in the efficiencies between data and simulation. These scale factors are derived using a tag-and-probe method in Z+jets events for light-flavored jets and in t̄t events for heavy-flavored jets. A further description of this tag-and-probe method can be found in Ref. [24]. A second algorithm is used to identify jets originating from c quarks [24]. This c tagging algorithm exploits information from displaced tracks, secondary vertices and soft leptons inside jets into a multivariate classifier, similar to that of the CSVv2 b tagging algorithm.

3.2 Event selection requirements

The analysis focuses on final-state signatures corresponding to a Higgs boson decay into a pair of b quarks and a leptonically decaying top quark: b-tagged jets and one isolated charged lepton. The charged lepton can either be an electron or a muon; τ leptons are included indirectly through their decays to their lighter siblings. In addition to this “lepton+jets” selection, the analysis makes use of an orthogonal data set, which is enriched in t̄t events, to better understand the t̄t background contribution. Five different categories of t̄t production with additional light-flavored (t̄t+LF) or heavy-flavored (t̄t+HF) jets are defined and treated separately: t̄t+LF, t̄t+c̄c, t̄t+b̄b, t̄t+b and t̄t+2b. The t̄t+2b category describes events where two b quarks are clustered into one single jet, which often happens with b quarks originating from gluon splitting. The contributions from these five categories to the overall t̄t BG are determined in events with two isolated electrons or muons (“dilepton” selection). As the flavor mixture of the additional jets does not depend on the decay of the W bosons from the top quark decays, the results obtained in the dilepton data set are used to constrain the flavor content of additional jets in t̄t production in the lepton+jets signal regions.

In the following subsections the selection criteria for the lepton+jets and dilepton selection are detailed.

3.2.1 Lepton+jets selection

Triggers and offline selection criteria are applied requiring an event to have exactly one muon (electron) candidate, that needs to fulfill $p_T > 27$ GeV ($p_T > 35$ GeV) and $|\eta| < 2.4$ ($|\eta| < 2.1$) in the muon (electron) channel and that is not produced inside jets. If an additional lepton exists that passes softer momentum requirements, i.e. $p_T > 15$ GeV, the event is rejected to suppress the contribution of Drell–Yan and of other processes that produce several prompt leptons. All central jets ($|\eta| < 2.4$) need to satisfy $p_T > 30$ GeV, while jets in the forward region ($2.4 \leq |\eta| \leq 4.7$) are required to have $p_T > 40$ GeV to ensure sufficiently good modeling of their kinematic properties. As the fourth b quark in the event, which originates from the initial gluon splitting, is typically produced with a softer p_T spectrum than the other quarks, the corresponding jet might not satisfy the jet p_T requirement. For this reason, two signal

regions are defined, which are based on the total number of jets and b-tagged jets in the event. The 3-tag region contains exactly three b-tagged jets and the 4-tag region exactly four b-tagged jets; both regions contain at least one additional untagged jet. Due to the detector geometry, only central jets can be b-tagged. By requiring at least three b-tagged jets the amount of QCD multijet events and W+jets events is significantly reduced with only a moderate impact on the signal. A missing transverse momentum (p_T^{miss}) selection is applied to further reject QCD multijet events, with thresholds optimized per channel: $p_T^{\text{miss}} > 35 \text{ GeV}$ in the muon channel and $p_T^{\text{miss}} > 45 \text{ GeV}$ in the electron channel. As the QCD multijet contribution is then reduced to a negligible level, this background is not considered in the analysis.

3.2.2 Dilepton selection

Several selection criteria are applied to obtain a dileptonic sample that contains similar numbers of dileptonic $t\bar{t}$ events with additional light-flavored jets, $t\bar{t}$ events with additional charm-flavored jets, and $t\bar{t}$ events with additional bottom-flavored jets. This sample is used to constrain the $t\bar{t} +$ heavy flavor rate uncertainties in the final fitting procedure. An event contains exactly two leptons that satisfy $p_T > 20 \text{ GeV}$ and $|\eta| < 2.4$; only for electrons, the subleading electron is required to fulfill $p_T > 15 \text{ GeV}$. The following dileptonic channels are combined into one common channel: $e+e$, $\mu+\mu$, $e+\mu$ and $\mu+e$, where the first mentioned lepton is the one with higher transverse momentum. The corresponding events are selected by applying different triggers that require one of the two leptons to have a higher p_T threshold. To reject QCD multijet events, an overall cut of $p_T^{\text{miss}} > 40 \text{ GeV}$ is applied. Since the final state of the dileptonic $t\bar{t}$ process includes at least two bottom quarks, at least two b-tagged jets are required. Furthermore, at least one additional jet with $p_T > 30 \text{ GeV}$ and $|\eta| < 2.4$ needs to fulfill the loose working point of the CSVv2 algorithm in order to obtain a comparable number of events $t\bar{t}+c\bar{c}$, $t\bar{t}+LF$ and for the $t\bar{t}$ processes that contain additional b jets. This working point provides a tagging efficiency of about 83% for b jets with a misidentification probability of approximately 10% for light-flavored jets or jets from gluons [24].

Table 1 provides a summary of the expected yields of the signal and background processes for the three regions considered (lepton+jets 3-tag, lepton+jets 4-tag, dilepton) after the full set of event selection criteria has been applied. For the signal processes, the yields are given for the SM and for the ITC cases.

4 Analysis strategy

The analysis searches for tH production with $H \rightarrow b\bar{b}$ and leptonic top quark decays in proton-proton collisions. The final-state topology is given by one charged lepton, missing transverse momentum, and multiple quarks, which hadronize to jets in the detector. The dominant background for tH(bb) production arises from various $t\bar{t}$ production processes due to the higher cross section and a similar final state, if one top quark decays leptonically and one top quark decays hadronically. A good understanding of this main background contribution is therefore crucial to the analysis.

With the help of boosted decision trees (BDTs), implemented in TMVA [25], the reconstructed jets of each event are assigned to hypothetical final-state quarks. Since the kinematic distributions and number of final-state quarks depend on the underlying event hypothesis, a dedicated jet assignment BDT (hereafter referred to as “JA-BDT”) is trained for each of the three hypotheses: tHQ signal process, tHW signal process, and $t\bar{t}$ background process.

Variables derived from the jet assignments and global event variables are combined by means

Table 1: Event yields for tHq and tHW signal (for the SM and ITC scenarios) as well as the various background processes in the two signal regions and in the dileptonic region. The uncertainties include both systematic and statistical uncertainties. Additionally, the numbers of observed events in data are shown.

	3-tag	4-tag	dilep
t <bar>t>+LF</bar>	24127 ± 5812	320 ± 181	5248 ± 998
t <bar>t>+c<bar>c</bar></bar>	8521 ± 4869	339 ± 256	2084 ± 1204
t <bar>t>+b<bar>b</bar></bar>	4115 ± 2265	777 ± 429	745 ± 436
t <bar>t>+b</bar>	3946 ± 2116	183 ± 113	766 ± 427
t <bar>t>+2b</bar>	2299 ± 1148	138 ± 88	401 ± 228
Single top	1979 ± 353	78.4 ± 25.8	285 ± 37
t <bar>t>Z</bar>	202 ± 30	32.0 ± 6.6	54.8 ± 7.3
Z+jets	—	—	69.0 ± 31.5
t <bar>t>W</bar>	90.3 ± 22.8	4.2 ± 2.8	31.4 ± 5.9
tZq	28.3 ± 5.7	2.9 ± 2.3	—
Sum of Backgrounds	45308 ± 8279	1875 ± 551	9684 ± 1695
t <bar>t>H</bar>	268 ± 31	62.0 ± 9.9	48.9 ± 5.9
tHq (SM)	11.1 ± 3.3	1.3 ± 0.3	0.31 ± 0.08
tHW (SM)	7.6 ± 1.1	1.1 ± 0.3	1.4 ± 0.2
tHq (ITC)	160 ± 38	19.1 ± 5.2	3.9 ± 1.0
tHW (ITC)	91.9 ± 11.9	13.7 ± 2.3	17.6 ± 2.2
Observed	44311	2035	9065

of a signal classification BDT (SC-BDT) which classifies each event that passes the lepton+jets selection into signal or background. Additionally, a dedicated BDT (flavor classification BDT, hereafter referred to as “FC-BDT”) is used to further constrain the contributions of different categories of the dominant tt> background by exploiting additional information from events passing the dilepton selection.

The two classifier output distributions of the SC-BDT (3-tag region and 4-tag region) are then used, together with the output distribution of the FC-BDT, to derive upper limits on the cross section of the production of Higgs bosons in association with top quarks. Limits are set on the tH production cross section for two dedicated scenarios, SM and ITC. To study the coupling of the Higgs boson to the top quark in a more general way, limits are also set on the combined cross sections for tH and tt>H production for various values for κ_t/κ_V . Although not sensitive to the relative sign between κ_t and κ_V , the tt>H process improves the sensitivity to the absolute value of the ratio of couplings significantly when treated as additional signal process.

5 Jet assignment

For each of the three considered final-state hypotheses (tHq, tHW, tt>), several jet assignments are possible per event. The number of permutations is reduced using b tagging information of the jets. For the tt> jet assignment, the jets assigned to the b quarks of the top quark decays are required to have a b tag. For the tHq and tHW jet assignments, the jets assigned to the b quarks have to be within the tracker acceptance, which corresponds to $|\eta| < 2.4$. Additionally, for the tHq jet assignment, the jet assigned to the quark that recoils against the W boson has to be untagged.

To find the best possible jet assignment for each event for each of the three hypotheses, JA-BDTs

are used. These BDTs are trained to discriminate between correct and incorrect assignments. Therefore in the training each event is reconstructed with both the best possible jet assignment and with one randomly chosen incorrect jet assignment. The correct jet assignment is the one that yields the lowest sum of all $\Delta R = \sqrt{\Delta\eta^2 + \Delta\phi^2}$ between the final-state quark and the assigned jet. For all jet assignments $\Delta R \leq 0.3$ must hold to be considered as a correct assignment. All other assignments are considered incorrect. Events with no possible correct assignment are not used in the training. The BDT is trained in a way that the highest response defines the best possible jet assignment. Therefore, the jet assignment with the highest JA-BDT response is chosen in the analysis.

The tHq and tHW JA-BDTs are trained on the ITC sample since it provides the largest number of events. The JA-BDTs use the kinematics and b tagging values of the final state particles as well as the angular variables between the jets of the Higgs boson or top quark decay.

6 Event classification

The second kind of BDTs used in the analysis are classification BDTs, which are used to classify the events as signal- and background-like.

6.1 Signal classification

The SC-BDT uses variables provided by the jet assignments together with assignment-independent variables to discriminate signal from background events. A list of all variables used in the training can be found in Table 2. The training is performed in the 3-tag region on a dedicated training sample, which is not used further in the analysis. The SC-BDT is trained with tHq and tHW events as signal and $t\bar{t}$ events as background contributions. As with the JA-BDTs, the SC-BDT is trained on the ITC sample. The trained BDT is then applied to the 3-tag and 4-tag regions.

In Figure 3 the output distribution of the SC-BDT is shown for signal and background processes.

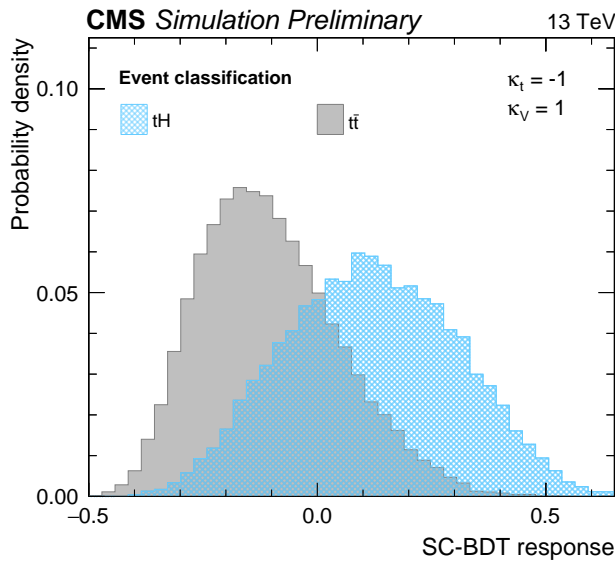


Figure 3: Output values of the SC-BDT.

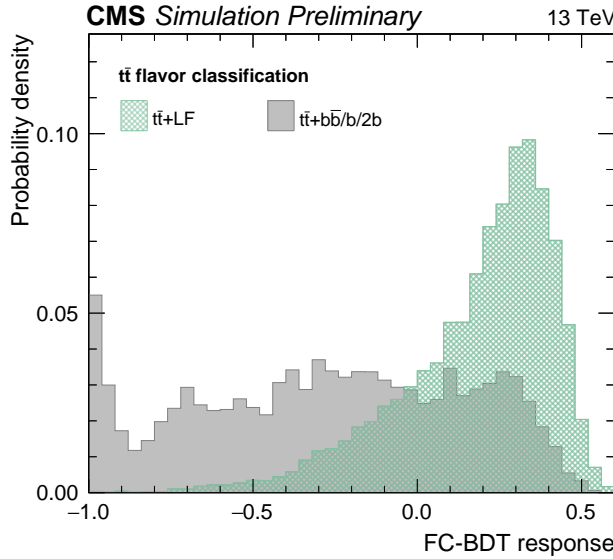


Figure 4: Response values of the FC-BDT. The background consists of $t\bar{t}+b\bar{b}$, $t\bar{t}+1\bar{b}$ and $t\bar{t}+2\bar{b}$ events.

6.2 Flavor classification

A dedicated FC-BDT is trained in the dileptonic region to discriminate $t\bar{t}$ events with additional light-flavored jets from $t\bar{t}+1b$, $t\bar{t}+2b$, and $t\bar{t}+b\bar{b}$ events. The $t\bar{t}+LF$ process is treated as signal in the training, while the $t\bar{t}$ processes that contain additional b jets are treated as background.

For the training of the $t\bar{t}$ FC-BDT, eight input variables are used. A description of these variables can be found in Table 3. In order to properly discriminate the $t\bar{t}+c\bar{c}$ process, which is neither considered as signal nor as background in the training, from the other processes, a dedicated charm-jet tagger [24] is used. As the properties of c jets are often distributed in between of those of b jets and light-flavored jets, a distinction between “charm-vs-light” (CvsL) and “charm-vs-bottom” (CvsB) is required.

The $t\bar{t}$ FC-BDT response (see Fig. 4) shows a clear separation between events with additional light-flavored jets and events with additional b jets. The output of the $t\bar{t}$ FC-BDT is applied to simulation and data events in the dileptonic region. It is then used in the final fit to constrain the normalization uncertainties on the $t\bar{t}$ processes.

Table 2: Description of variables used in the SC-BDT. There are four types of variables: variables independent of any jet assignment, and variables based on objects obtained under the $t\bar{t}$, tHq, or tHW jet assignment. The logarithm transformation is used to smooth and constrain broad distributions to a more narrow range.

Variable	Description
Event variables	
$\log m_3$	invariant mass of three hardest jets in the event
aplanarity	aplanarity of the event
Fox-Wolfram #1	first Fox-Wolfram moment of the event
$q(\ell)$	electric charge of the lepton
$t\bar{t}$ jet assignment variables	
$\log m(t_{\text{had}})$	invariant mass of the reconstructed hadronically decaying top quark
$\text{CSV}(W_{\text{had}} \text{ jet } 2)$	output of the b tagging discriminant for the second jet assigned to the hadronically decaying W boson
$\text{CSV}(W_{\text{had}} \text{ jet } 1)$	output of the b tagging discriminant for the first jet assigned to the hadronically decaying W boson
$\Delta R(W_{\text{had}} \text{ jets})$	ΔR between the two light jets assigned to the hadronically decaying W boson
tHq jet assignment variables	
$\log p_T(\text{Higgs})$	transverse momentum of the reconstructed Higgs boson candidate
$ \eta(\text{light jet}) $	absolute pseudorapidity of light forward jet
$\log m(\text{Higgs})$	invariant mass of the reconstructed Higgs boson candidate
$\text{CSV}(\text{Higgs jet } 1)$	output of the b tagging discriminant for the first jet assigned to the Higgs boson candidate
$\text{CSV}(\text{Higgs jet } 2)$	output of the b tagging discriminant for the second jet assigned to the Higgs boson candidate
$\cos \theta(b_t, \ell)$	cosine of the angle between the b-tagged jet from the top quark decay and the lepton.
$\cos \theta^*$	cosine of the angle between the light forward jet and the lepton in the top quark rest frame
$ \eta(t) - \eta(H) $	absolute pseudorapidity difference of reconstructed Higgs boson and reconstructed top quark
$\log p_T(\text{light jet})$	transverse momentum of the light forward jet
tHW jet assignment variable	
JA-BDT response	best output of the tHW JA-BDT

Table 3: Input variables used in the training of the FC-BDT. The variables are sorted by their importance in the training within each category.

Variable	Description
CSV(b jet 3)	output of the b tagging discriminant for the b-tagged jet with the third highest b tagging value in the event
$n_{\text{jets}}(\text{tight})$	number of jets in the event passing the tight working point of the b tagging algorithm
CvsL(jet p_T 3)	output of the charm vs. light flavor tagging algorithm for the jet with the third highest transverse momentum in the event
CSV(b-tagged jet 2)	output of the b tagging discriminant for the b-tagged jet with the second highest b tagging value in the event
CvsL(jet p_T 4)	output of the charm vs. light flavor tagging algorithm for the jet with the fourth highest transverse momentum in the event
CvsB(jet p_T 3)	output of the charm vs. bottom flavor tagging algorithm for the jet with the third highest transverse momentum in the event
CSV(b-tagged jet 4)	output of the b tagging discriminant for the b-tagged jet with the fourth highest b tagging value in the event
$n_{\text{jets}}(\text{loose})$	number of jets in the event passing the loose working point of the b tagging algorithm

7 Systematic uncertainties

There are a number of systematic uncertainties that affect the results of this analysis. These uncertainties can be grouped into experimental and theoretical uncertainties and those further into normalization and shape uncertainties depending on how they affect the output of the SC-BDT and FC-BDT. The uncertainties are parametrized as nuisance parameters in the statistical inference performed in the final analysis step.

The uncertainty on the measurement of the luminosity (2.5% [26]) affects the normalization of all processes. Systematically shifted event weights are used in the simulation to account for uncertainties in the estimation of the corrected lepton efficiencies. The uncertainty in the distribution of the number of pileup interactions is applied by varying the cross section used to predict the number of pileup interactions in the simulation by $\pm 4.6\%$ from its nominal value of 69.2 mb. A smearing of the jet four-momenta is applied to account for the known differences in jet energy resolution between simulation and data. The applied jet energy corrections are varied within their uncertainties and are considered for different uncertainty sources. In addition, the contributions to p_T^{miss} from particles with low transverse momentum that have not been clustered into jets are varied within their respective energy resolutions [27]. The evaluation of the systematic uncertainties on the CSVv2 b tagging scale factors follows the procedure of Ref. [28]. Differential measurements of the top quark p_T spectrum in $t\bar{t}$ events [29] have shown that a softer spectrum is observed than predicted. To account for this discrepancy, the results derived using the default simulation for $t\bar{t}$ are compared to the results using simulated $t\bar{t}$ events that are reweighted according to the observed difference between data and simulation in Ref. [29]. This is then used to estimate the systematic uncertainty on the nominal $t\bar{t}$ sample.

A 50% normalization uncertainty is assigned for the $t\bar{t}+\text{HF}$ categories, as neither higher-order theoretical calculations nor control region studies are able to constrain the normalization of these processes to better than 50%.

Simulation samples with halved or doubled values of the nominal factorization and renormalization scales (μ_R , μ_F) at the matrix element are emulated with a LHE reweighting procedure. These weights are not available for the single top samples. Therefore the single top samples are assigned a 3.0% normalization uncertainty to cover the effect of the variation of these scales. Uncertainties from the shape of the parton distribution functions (PDF) in the simulation are considered only as normalization uncertainties since the shape variations have been found to be negligible.

Table 4 shows the shift of the fitted tH signal strength for the ITC scenario if all nuisance parameters associated with a given group of uncertainties are frozen to their nominal value during the fitting procedure. The dominant systematic uncertainties arise from the normalization of the $t\bar{t}+\text{HF}$ categories, b tagging, and the jet energy scale.

8 Results

The upper asymptotic CL_S limits [30] on cross sections times branching ratio at 95% CL are calculated by performing a simultaneous maximum-likelihood fit on the SC-BDT response in the 3-tag and 4-tag regions and on the FC-BDT response in the dileptonic region. The distributions before performing the fit are displayed in Fig. 5; in Fig. 6 these distributions are shown after the fit. Assuming only tH production as signal and $t\bar{t}H$ as background, the upper limit is found to be $89.5 \times \sigma_{\text{SM}}$ (41.4 expected) for the SM scenario and $5.83 \times \sigma_{\text{ITC}}$ (2.94 expected) for the ITC scenario. This corresponds to observed (expected) upper limits on the cross section of

Table 4: Shift of the fitted tH signal strength for the ITC scenario if the nuisance parameters of the given set are frozen to their nominal values during the fit.

Nuisance parameters	Shift of signal strength in %
t̄t + HF	9.2
b tagging	7.5
JES	-5.3
MC sample size	3.1
pileup	1.8
QCD scale	1.4
top p_T	-0.8
lepton efficiencies	0.4
luminosity	-0.4
JER	0.3
PDF	0.2
unclustered energy	0.2

4.65 pb (2.15 pb) for the SM scenario and 3.36 pb (1.69 pb) for the ITC scenario. The expected and observed upper limits on the combined cross section times the branching ratio of the tHq, tHW, and t̄tH processes for different values of the coupling ratios κ_t/κ_V can be found in Fig. 7. The different scenarios are implemented using the reweighting procedure as described in Section 2.

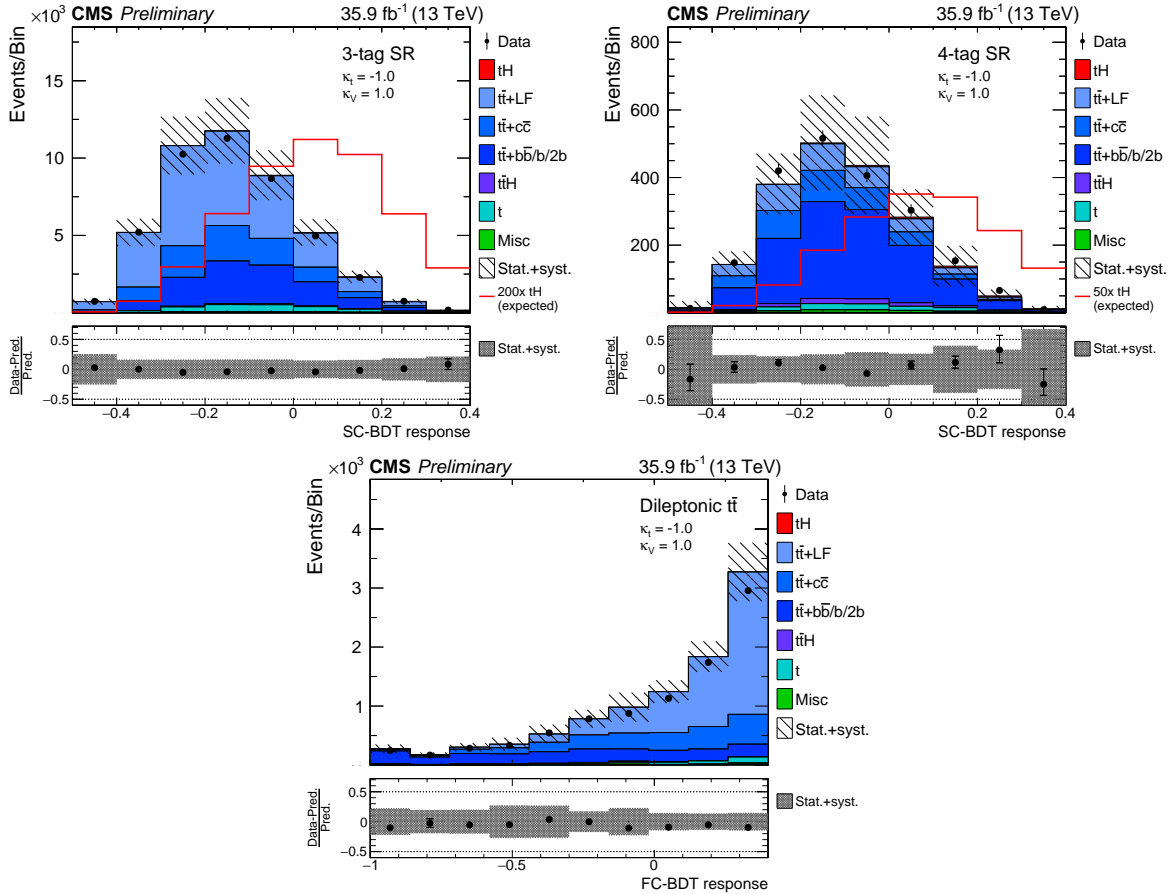


Figure 5: Prefit distributions of the output of the SC-BDT in the 3-tag and 4-tag regions, as well as the output of the FC-BDT in the dileptonic region. The red lines indicate the expected signal contributions scaled by the factors given in the legends. Underflow and overflow events are included in the first and last bin, respectively.

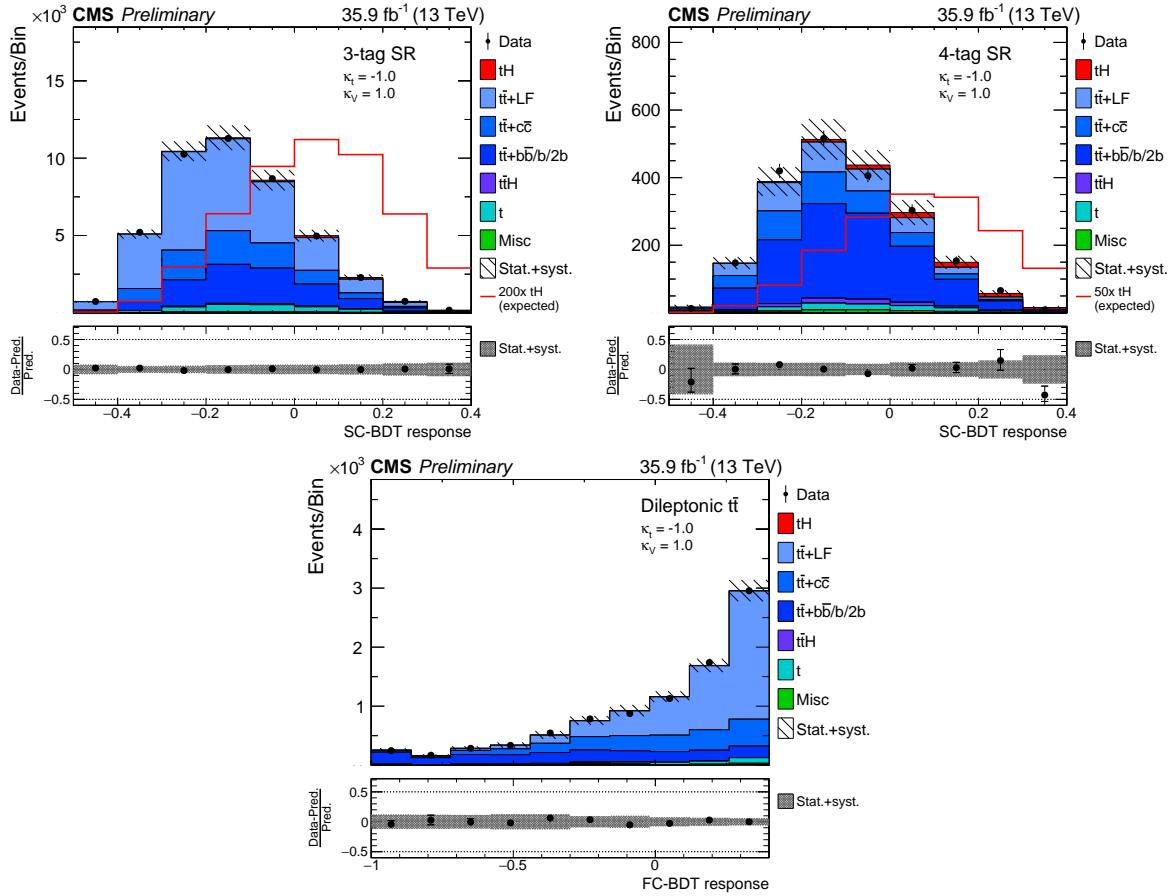


Figure 6: Postfit distributions of the output of the SC-BDT in the 3-tag and 4-tag regions, as well as the output of the FC-BDT in the dileptonic region, corresponding to the limit setting on $t\bar{t}H$ production in the ITC case. The red lines indicate the expected signal contributions scaled by the factors given in the legends. Underflow and overflow events are included in the first and last bin, respectively.

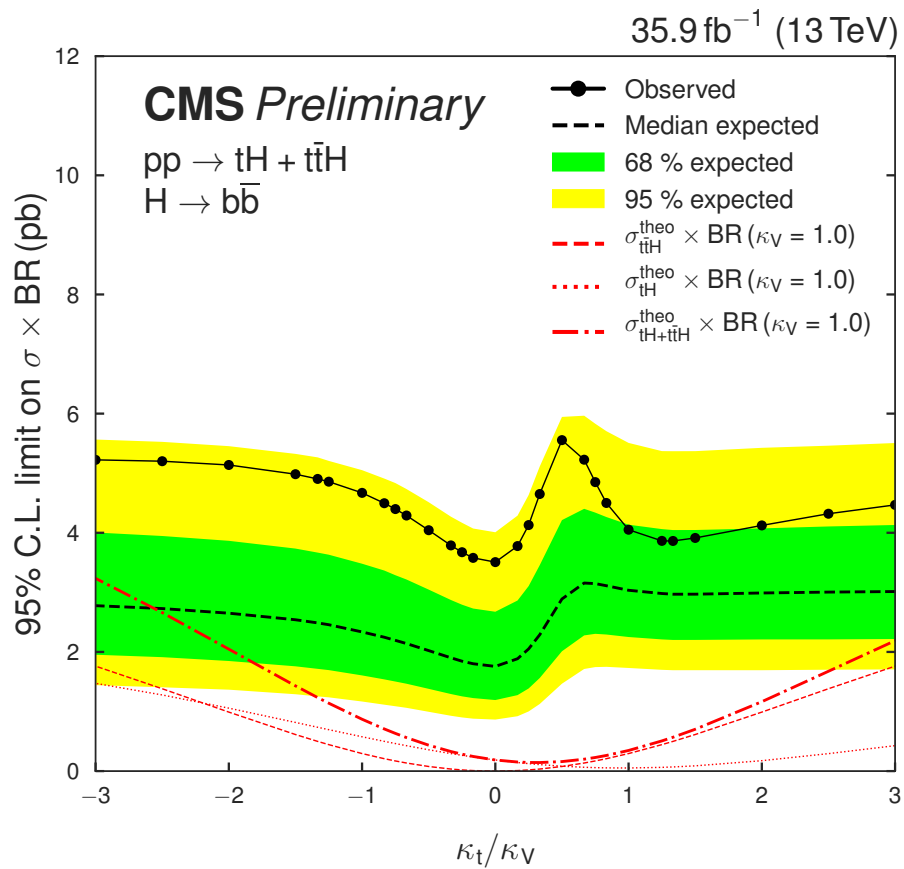


Figure 7: Upper limits on $tH + t\bar{t}H$ scenarios with different κ_t/κ_V ratios. The red lines show the theory predictions and the inner (green) band and the outer (yellow) band indicate the regions containing 68 and 95%, respectively, of the distribution of limits expected under the background-only hypothesis. None of the inspected points can be excluded.

9 Summary

A search for Higgs boson production in association with single top quarks (tH) in the t - and the tW -channel production mode has been presented in this document with a focus on possible variations in the coupling between the Higgs boson and the top quark or the W boson to search for deviations from the standard model. The full 2016 dataset of the CMS detector with an integrated luminosity of 35.9 fb^{-1} at a center-of-mass energy of 13 TeV has been analyzed. The observed (expected) upper limits for tH production are found to be $89.5 \times \sigma_{\text{SM}}$ ($41.4 \times \sigma_{\text{SM}}$) for the standard model scenario and $5.83 \times \sigma_{\text{ITC}}$ ($2.94 \times \sigma_{\text{ITC}}$) for the inverted top coupling scenario, where σ_{SM} and σ_{ITC} are the predicted cross sections in these two scenarios. In addition, the upper limits on the combined cross section for tH production and the production of a Higgs boson in association with a pair of top quark and antiquark for various values of the ratio of the coupling strength factors κ_t/κ_V are determined. With the available data set, it is not possible to exclude any of the scenarios with this analysis.

References

- [1] CMS Collaboration, “Observation of a new boson at a mass of 125 GeV with the CMS experiment at the LHC”, *JHEP* **06** (2013) 081, doi:10.1007/JHEP06(2013)081.
- [2] ATLAS Collaboration, “Observation of a new particle in the search for the Standard Model Higgs boson with the ATLAS detector at the LHC”, *Phys. Lett. B* **716** (2012) 1, doi:10.1016/j.physletb.2012.08.020, arXiv:1207.7214.
- [3] CMS Collaboration, “Observation of $t\bar{t}H$ production”, (2018). arXiv:1804.02610. Submitted to *Phys. Rev. Lett.*
- [4] S. Biswas, E. Gabrielli, and B. Mele, “Single top and Higgs associated production as a probe of the $Ht\bar{t}$ coupling sign at the LHC”, *JHEP* **01** (2013) 088, doi:10.1007/JHEP01(2013)088, arXiv:1211.0499.
- [5] B. Hespel, F. Maltoni, and E. Vryonidou, “Higgs and Z boson associated production via gluon fusion in the SM and the 2HDM”, *JHEP* **06** (2015) 065, doi:10.1007/JHEP06(2015)065, arXiv:1503.01656.
- [6] CMS Collaboration, “Precise determination of the mass of the Higgs boson and tests of compatibility of its couplings with the standard model predictions using proton collisions at 7 and 8 TeV”, *Eur. Phys. J. C* **75** (2015), no. 5, 212, doi:10.1140/epjc/s10052-015-3351-7, arXiv:1412.8662.
- [7] ATLAS and CMS Collaborations, “Measurements of the Higgs boson production and decay rates and constraints on its couplings from a combined ATLAS and CMS analysis of the LHC pp collision data at $\sqrt{s} = 7$ and 8 TeV”, *JHEP* **08** (2016) 045, doi:10.1007/JHEP08(2016)045, arXiv:1606.02266.
- [8] CMS Collaboration, “Combined measurements of the Higgs boson’s couplings at $\sqrt{s} = 13$ TeV”, CMS Physics Analysis Summary CMS-PAS-HIG-17-031, CERN, Geneva, 2018.
- [9] J. Ellis and T. You, “Updated Global Analysis of Higgs Couplings”, *JHEP* **06** (2013) 103, doi:10.1007/JHEP06(2013)103, arXiv:1303.3879.
- [10] F. Demartin, F. Maltoni, K. Mawatari, and M. Zaro, “Higgs production in association with a single top quark at the LHC”, *Eur. Phys. J. C* **75** (2015), no. 6, 267, doi:10.1140/epjc/s10052-015-3475-9.
- [11] J. Alwall et al., “The automated computation of tree-level and next-to-leading order differential cross sections, and their matching to parton shower simulations”, *JHEP* **07** (2014) 079, doi:10.1007/JHEP07(2014)079, arXiv:1405.0301.
- [12] F. Demartin et al., “ tWH associated production at the LHC”, *Eur. Phys. J. C* **77** (2017), no. 1, 34, doi:10.1140/epjc/s10052-017-4601-7.
- [13] NNPDF Collaboration, “Parton distributions for the LHC Run II”, *JHEP* **04** (2015) 040, doi:10.1007/JHEP04(2015)040, arXiv:1410.8849.
- [14] T. Sjöstrand et al., “An Introduction to PYTHIA 8.2”, *Comput. Phys. Commun.* **191** (2015) 159–177, doi:10.1016/j.cpc.2015.01.024, arXiv:1410.3012.

- [15] P. Nason, “A New Method for Combining NLO QCD with Shower Monte Carlo Algorithms”, *JHEP* **11** (2004) 040, doi:10.1088/1126-6708/2004/11/040, arXiv:hep-ph/0409146.
- [16] S. Frixione, P. Nason, and C. Oleari, “Matching NLO QCD computations with Parton Shower simulations: the POWHEG method”, *JHEP* **11** (2007) 070, doi:10.1088/1126-6708/2007/11/070, arXiv:0709.2092.
- [17] S. Alioli, P. Nason, C. Oleari, and E. Re, “A general framework for implementing NLO calculations in shower Monte Carlo programs: the POWHEG BOX”, *JHEP* **06** (2010) 043, doi:10.1007/JHEP06(2010)043, arXiv:1002.2581.
- [18] R. Frederix and S. Frixione, “Merging meets matching in MC@NLO”, *JHEP* **12** (2012) 061, doi:10.1007/JHEP12(2012)061, arXiv:1209.6215.
- [19] GEANT4 Collaboration, “GEANT4: A Simulation toolkit”, *Nucl. Instrum. Meth. A* **506** (2003) 250, doi:10.1016/S0168-9002(03)01368-8.
- [20] J. Allison et al., “Geant4 developments and applications”, *IEEE Transactions on Nuclear Science* **53** (2006), no. 1, 270, doi:10.1109/TNS.2006.869826.
- [21] CMS Collaboration, “Particle-flow reconstruction and global event description with the cms detector”, *JINST* **12** (2017) P10003, doi:10.1088/1748-0221/12/10/P10003, arXiv:1706.04965.
- [22] M. Cacciari, G. P. Salam, and G. Soyez, “The anti- k_t jet clustering algorithm”, *JHEP* **04** (2008) 063, doi:10.1088/1126-6708/2008/04/063, arXiv:0802.1189.
- [23] CMS Collaboration, “Jet energy scale and resolution in the CMS experiment in pp collisions at 8 TeV”, *JINST* **12** (2017), no. 02, P02014, doi:10.1088/1748-0221/12/02/P02014, arXiv:1607.03663.
- [24] CMS Collaboration, “Identification of heavy-flavour jets with the CMS detector in pp collisions at 13 TeV”, (2017). arXiv:1712.07158. Submitted to *JINST*.
- [25] A. Hoecker et al., “TMVA - Toolkit for Multivariate Data Analysis”, (2007) arXiv:physics/0703039.
- [26] CMS Collaboration, “CMS Luminosity Measurement for the 2016 Data Taking Period”, CMS Physics Analysis Summary CMS-PAS-LUM-17-001, CERN, Geneva, 2017.
- [27] CMS Collaboration, “Performance of the CMS missing transverse momentum reconstruction in pp data at $\sqrt{s} = 8$ TeV”, *JINST* **10** (2015), no. 02, P02006, doi:10.1088/1748-0221/10/02/P02006, arXiv:1411.0511.
- [28] CMS Collaboration, “Search for $t\bar{t}H$ production in the $H b\bar{b}$ decay channel with leptonic $t\bar{t}$ decays in proton-proton collisions at $\sqrt{s} = 13$ TeV”, (2018). arXiv:1804.03682. Submitted to *JHEP*.
- [29] CMS Collaboration, “Measurement of the differential cross section for top quark pair production in pp collisions at $\sqrt{s} = 8$ TeV”, *Eur. Phys. J. C* **75** (2015), no. 11, 542, doi:10.1140/epjc/s10052-015-3709-x, arXiv:1505.04480.
- [30] G. Cowan, K. Cranmer, E. Gross, and O. Vitells, “Asymptotic formulae for likelihood-based tests of new physics”, *Eur. Phys. J. C* **71** (2011) 1554, doi:10.1140/epjc/s10052-011-1554-0, 10.1140/epjc/s10052-013-2501-z, arXiv:1007.1727. [Erratum: Eur. Phys. J.C73,2501(2013)].